Published in final edited form as:

Ultrasound Med Biol. 2016 January ; 42(1): 257–271. doi:10.1016/j.ultrasmedbio.2015.08.018.

Design and characterization of fibrin-based acoustically responsive scaffolds for tissue engineering applications

Alexander Moncion[1,2], **Keith J. Arlotta**[2], **Oliver D. Kripfgans**[1,2,3], **J. Brian Fowlkes**[1,2,3], **Paul L. Carson**[1,2,3], **Andrew J. Putnam**[3], **Renny T. Franceschi**[3,4,5], and **Mario L. Fabiilli**[1,2]

[1]Applied Physics Program, University of Michigan, Ann Arbor, MI USA

[2]Department of Radiology, University of Michigan Health System, Ann Arbor, MI USA

[3]Department of Biomedical Engineering, University of Michigan, Ann Arbor, MI USA

[4]School of Dentistry, University of Michigan, Ann Arbor, MI USA

[5]Department of Biological Chemistry, University of Michigan Medical School, Ann Arbor, MI USA

Abstract

Hydrogel scaffolds are used in tissue engineering as a delivery vehicle for regenerative growth factors (GFs). Spatiotemporal patterns of GF signaling are critical for tissue regeneration, yet most scaffolds afford limited control of GF release, especially after implantation. We previously demonstrated that acoustic droplet vaporization (ADV) can control GF release from a fibrin scaffold doped with a perfluorocarbon emulsion. This study investigates properties of the acoustically responsive scaffold (ARS) critical for further translation. At 2.5 MHz, ADV and inertial cavitation thresholds ranged from 1.5 – 3.0 MPa and 2.0 – 7.0 MPa peak rarefactional pressure, respectively, for ARSs of varying compositions. Viability of C3H10T1/2 cells, encapsulated in the ARS, did not decrease significantly for pressures below 4 MPa. ARSs with perfluorohexane emulsions displayed higher stability versus perfluoropentane emulsions, while surrogate payload release was minimal without ultrasound. These results enable the selection of ARS compositions and acoustic parameters needed for optimized spatiotemporal control.

Keywords

acoustic droplet vaporization; inertial cavitation; ultrasound; spatiotemporal drug delivery; controlled release; emulsion; perfluorocarbon; fibrin

Corresponding Author: Alexander Moncion, M.S, University of Michigan, 3225 Medical Sciences Building I, 1301 Catherine Street, Ann Arbor, MI 48109-5667, Phone: 305-546-6496, ambaez@umich.edu.

Introduction

Fibrin scaffolds are highly porous, protein-based hydrogels frequently used in regenerative medicine as a substrate for cells and for encapsulation of proteins such as growth factors (GFs) (Shaikh et al. 2008; Dehghani and Annabi 2011; Seliktar 2012). Similar to other hydrogels, the release of a bioactive molecule (i.e., payload) from a conventional fibrin scaffold as well as degradation of the scaffold are dominated by processes such as molecular diffusion, material degradation, and cell migration. Thus the rate that biochemical (e.g., GFs) or mechanical (e.g., microporosity) cues are presented in a conventional fibrin scaffold cannot be externally controlled spatially or temporally, especially after the scaffold is implanted *in vivo*. It is well documented that spatial and temporal patterns of GF signaling are critically important in regenerative processes (Bos et al. 2001; Sojo et al. 2005); additionally, cellular processes are influenced by the mechanical properties of the local scaffold microenvironment (Metallo et al. 2007; Tse et al. 2012; Barthes et al. 2014; Fujie et al. 2014; Satyam et al. 2014). Alternatively, scaffolds have been designed to respond to environmental or externally applied stimuli - such as light, electricity, magnetic fields, temperature, enzymes, and pH – in order to obtain spatiotemporal control of payload release or to modify scaffold architecture after implantation (Sakiyama-Elbert and Hubbell 2000b; Sakiyama-Elbert and Hubbell 2000a; Matsusaki and Akashi 2005; Thornton et al. 2005; Frimpong et al. 2007; Kulkarni and Biswanath 2007; Lavigne et al. 2007; Wu et al. 2008; Zhao et al. 2011). Despite their promising potential in controlling both biochemical and mechanical cues, further development of responsive scaffolds is limited in part by the clinical translatability of the modulating stimulus, especially in terms of focusing the stimulus or targeting deeply located scaffolds.

Ultrasound (US) has been explored as a stimulus for achieving spatial and temporal control with responsive scaffolds due to its potential for translatability. Unlike other stimuli, US can be applied non-invasively, focused with submillimeter precision, and penetrate deep within the body. Broadly, US can be used to generate mechanical and/or thermal effects within a scaffold to achieve on-demand control. In many instances, US-responsive scaffolds contain sonosensitive particles such as emulsions or microbubbles, thus making the scaffold more responsive to US (Epstein-Barash et al. 2010; Fabiilli et al. 2013). However, it has been demonstrated using low frequency US that payload release can be modulated from scaffolds in the absence of sonosensitive particles (Huebsch et al. 2014). Sonosensitive particles are usually administered intravascularly for US-based imaging or therapy, with microbubbles used clinically as US contrast agents. These particles are typically micron-size in diameter, contain a perfluorocarbon (PFC) dispersed (i.e., core) phase, and are stabilized by a surfactant shell. Microbubbles, which contain a gaseous PFC core, have been used to indirectly facilitate payload delivery from an *in situ* cross-linking hydrogel containing liposomes co-encapsulated with the microbubbles (Epstein-Barash et al. 2010). In the absence of US, microbubbles have also been used to create on-demand, microporous agarose hydrogels (Lima et al. 2012) or to simultaneously act as a porogen and GF carrier within poly(lactic-co-glycolic-acid) scaffolds (Nair et al. 2010).

The presented studies build upon previous work where we demonstrated the utility of fibrin scaffolds doped with sonosensitive PFC emulsions, termed here acoustically responsive

scaffolds (ARSs). US was used to modulate GF release from the ARS as well as induce drastic changes in architecture and shear stiffness of the ARS (Fabiilli et al. 2013). Fibrin was chosen as the hydrogel in the ARS due to its widespread use within the field of tissue engineering as a delivery system for GFs, cells, drugs, and genes (Whelan et al. 2014). Sonosensitive PFC emulsions, with single or double structures, have been used as on-demand contrast agents and delivery vehicles for bioactive payloads, respectively (Kripfgans et al. 2000; Unger et al. 2004; Diaz-Lopez et al. 2010; Fabiilli et al. 2013; Javadi et al. 2013). The PFC within these emulsions transitions from a liquid into a gas when the emulsion is exposed to US above a specific acoustic amplitude. This phase transition is termed acoustic droplet vaporization (ADV) (Kripfgans et al. 2004) and occurs in a microsecond time frame (Fabiilli et al. 2010; Wong et al. 2011). PFCs such as perfluoropentane (PFP, C_5F_{12}, 29°C boiling point) and perfluorohexane (PFH, C_6F_{14}, 56°C boiling point) are typically used in sonosen sitive emulsions because of their biocompatibility and inertness. The emulsification process (i.e., formation of droplets) prevents low boiling point PFCs, like PFP, from vaporizing at homeostatic body temperature (37°C) due to an increase in Laplace pressure, which causes an elevation of the PFC boiling point within the droplets (Rapoport et al. 2009; Sheeran et al. 2011). Sonosensitive emulsions can possess both single and double emulsion structures. With single emulsions of the form PFC-in-water (PFC/W), the PFC is dispersed within an aqueous continuous phase. For delivery of payloads such as GFs, a secondary dispersed phase is added since PFCs are extremely hydrophobic and lipophobic. Thus double emulsions of the form water-in-PFC-in-water (W_1/PFC/W_2) have been used for GF delivery in ARSs whereby the GF is contained within the W_1 phase (Fabiilli et al. 2013).

For responsive scaffolds, the physicochemical properties of the scaffold are related to the manner in which the scaffold will respond to a stimulus. Conversely, the properties of the stimulus (e.g., intensity, duration, or directionality) impact the response of the scaffold. Thus, elucidating the mechanisms that occur when an ARS is exposed to US is critical in not only achieving optimal payload release from the scaffold, but also relevant for facilitating regenerative processes that could occur within or adjacent to the ARS. In addition to ADV, inertial cavitation (IC) has been observed when sonosensitive emulsions undergo a phase shift (Fabiilli et al. 2009). IC can occur when a bubble, either generated by ADV or the nucleation of dissolved gas, rapidly expands and collapses due to US exposure. This violent behavior by the bubble can generate very high temperatures and velocities at the bubble site, which can ultimately cause bioeffects such as cellular damage and sonoporation (Ferrara et al. 2007).

The presented *in vitro* work on a fibrin-based ARS is divided into three main parts. First, the ADV and IC thresholds were measured for ARSs of varying composition. Parameters such as fibrin density, emulsion formulation (including stabilizing shell, PFC core, and emulsion structure), and acoustic cycles were explored. Second, the viability of cells encapsulated in the ARS was evaluated across the different regimes of ADV and IC. Third, the physical stabilities of the ARSs, including non-selective (i.e., without US exposure) release profiles, were measured over the course of 7 days.

Materials and Methods

Single Emulsion Preparation and Characterization

Four different formulations of single emulsions (PFC/W) were made by combining 25% (v/v) PFP (CAS#: 678-26-2, Strem Chemicals, Newburyport, MA USA) or PFH (CAS#: 355-42-0, Strem Chemicals) and 75% (v/v) of an aqueous emulsifying agent. The aqueous phase consisted of either a lipid blend of 6.67 mg/mL 1,2-dipalmitoyl-*sn*-glycero-3-phosphocholine (DPPC, CAS#: 63-89-8 Avanti Polar Lipids, Inc., Alabaster, AL USA) and 0.27 mg/mL 1,2-dipalmitoyl-*sn*-glycero-3-phosphate monosodium salt (DPPA, CAS#: 169051-60-9, Avanti Polar Lipids, Inc) dissolved in a solution of propylene glycol (CAS#: 57-55-6, Sigma-Aldrich, St. Louis, MO USA), normal saline (Baxter Healthcare, Deerfield, IL USA), and glycerol (CAS#: 56-81-5, Sigma-Aldrich); 4 mg/mL bovine serum albumin (BSA) (CAS#: 9048-46-8, Sigma-Aldrich) dissolved in Dulbecco's phosphate buffered saline (DPBS, Life Technologies, Grand Island, NY USA); or 4 mg/mL Pluronic F68 (CAS#: 9003-11-6, Sigma-Aldrich) dissolved in DPBS. The fluids were shaken with an amalgamator (Wig-L-Bug, Sigma-Aldrich) at 4800 rpm for 90 seconds (Fabiilli et al. 2009). The resulting emulsions were stored at 5°C for 30 minutes and then subsequently washed with normal saline to remove excess emulsifier. The emulsions were characterized with a Coulter Counter (Multisizer 4, Beckman Coulter, Inc., Indianapolis, IN USA) in the range of 1-30 μm. All single emulsion formulations are listed in Table 1.

Double Emulsion Preparation and Characterization

Double emulsions (W_1/PFC/W_2) were prepared with PFP or PFH as the PFC phase by modifying a previous method (Fabiilli et al. 2010). A triblock fluorosurfactant, consisting of Krytox 157FSH (CAS# 51798-33-5, DuPont, Wilmington, DE, USA) and polyoxyethylene glycol (MW: 1000 g/mol, CAS#: 24991-53-5, Alfa Aeser, Ward Hill, MA USA), was dissolved in 1 g of PFC at 2% (w/w). The PFC solution was then combined with an aqueous solution of fluorescein sodium salt (FSS, CAS#: 518-47-8, Sigma-Aldrich), reconstituted at 1 mg/mL in DPBS, in a volumetric ratio of 2.1:1. The phases were sonicated (CL-188, QSonica, LLC, Newton, CT USA) for 30 seconds while on ice. The resulting primary emulsion (W_1/PFC) was added drop wise to a solution of 50 mg/mL Pluronic F68 in DPBS and stirred with a magnetic stir bar at 700 rpm for 2 minutes while on ice. The particle size of the resulting coarse double emulsion (W_1/PFC/W_2) was reduced using a homogenizer (T10, IKA Works Inc., Wilmington, NC USA). The resulting emulsion had a FSS encapsulation efficiency of 89.7% and 92.3% for the PFP and PFH formulations, respectively. Emulsions were stored at 5°C for 30 minutes and characterized with a Coulter Counter in the range of 1-30 μm. All double emulsion formulations are listed in Table 1.

ARS Fabrication

ARSs were prepared using 3, 5, or 10 mg/mL clottable protein by first combining bovine fibrinogen (Sigma-Aldrich), dissolved in degassed (40% O_2 saturation) Dulbecco's modified Eagle's medium (DMEM, Life Technologies), with bovine thrombin (2 U/mL, Thrombin-JMI, King Pharmaceuticals, Bristol, TN, USA), and 1% (v/v) emulsion. The mixture was injected into an OptiCell (Thermo Fisher Scientific Inc., Waltham, MA USA) and allowed

to polymerize for 30 min at room temperature. Hydrogels without emulsions were prepared as a sham condition.

Ultrasound Exposure

OptiCells containing the ARSs were fixed vertically in a tank of degassed water (30-36% O_2 saturation) at 37°C, as shown in Fig. 1-A. A calib rated, single element US transducer (2.5 MHz, H108, Sonic Concepts, Inc., Bothell, WA USA) was positioned such that the focus of the transducer was located equidistant from the OptiCell windows, which are 75 μm thick and spaced 2 mm apart. This single element transducer (f-number = 0.83, focal length = 50 mm) was used to generate ADV and IC within the ARS. Previous studies (Rahim et al. 2006a; Rahim et al. 2006b; Meijering et al. 2007) have demonstrated that OptiCell windows attenuate US in the range of 1-3 MHz by less than 1%. The ARS was exposed to 100 pulses of US that were 3, 6, or 13 acoustic cycles in length with a pulse repetition frequency (PRF) of 10 Hz and amplitudes ranging from 0.8 - 8 MPa peak rarefactional pressure. Waveforms were generated using a dual channel function generator (33500B, Agilent Technologies, Santa Clara, CA USA) and amplified by a gated radio frequency (RF) amplifier (GA-2500A Ritec Inc, Warwick, RI USA). Gating was realized using the second channel of the function generator. During exposure, broadband noise – indicative of IC (Madanshetty and Apfel 1991; Hwang et al. 2006) - was detected by a calibrated hydrophone (1-50 MHz, Onda Corporation, Sunnyvale, CA USA) that was coupled to the single element transducer and positioned 6 cm from the OptiCell. Hydrophone waveforms were digitized by an oscilloscope (HDO4034, Teledyne Lecroy, Chestnut Ridge, NY USA) at a sampling rate of 100 MHz. In order to detect bubble formation, B-mode US images were acquired before and after exposures from the single element transducer using a clinical US scanner (10 MHz US linear imaging array, 10L, GE Vivid 7, GE Healthcare, Waukesha, WI USA). To prevent the linear US array from generating ADV and/or IC within the ARS, a mechanical index (MI) of 0.03 was used, which is significantly lower than the MI required to cause cavitation (Apfel and Holland 1991). It was confirmed that this low MI caused no increase in echogenicity, and hence no ADV, in the ARS. For a given experimental run, which consisted of interrogating acoustic amplitudes in the range of 0.8 – 8.0 MPa peak rarefactional pressure, the spacing between each acoustic exposure in the OptiCell was 3 mm. This spacing minimized the interaction between exposure sites since the −6 dB lateral beam width of the single element transducer was measured as 0.61 mm. The minimum distance between an exposure and the edge of the OptiCell window was 10 mm. A total of 78 exposures was done per OptiCell with a separation of 10 mm between runs. All acoustic data (i.e., B-mode images and hydrophone data) were analyzed in MATLAB (The Mathworks Inc., Natick, MA USA). The B-mode images, before and after US exposure from the single element transducer, were subtracted and the mean echo power (MEP) was calculated for the subtracted image as done previously (Fabiilli et al. 2009). The ADV threshold was defined as P_n, where P_n was the first acoustic pressure that satisfied Eqn. 1,

$$MEP_n > \left(\sum_{i=1}^{n-1} MEP_i\right) / (n-1) + 3\sigma \quad (1)$$

where MEP_n was the MEP of the n^{th} pressure exposure, MEP_i was the MEP of the i^{th} pressure exposure, and σ was the standard deviation of MEP_1, MEP_2, MEP_3, ... MEP_{n-1}.

At each acoustic exposure condition, the RF signals collected using the hydrophone consisted of 100 segments, one for each of the 100 pulses fired by the single element transducer. A Hanning window was applied to each segment to time gate physical window reflections from the OptiCell and the direct path transmit signal from the single element transducer. Then the fast Fourier transform (FFT) of each segment was computed. Fundamental as well as second and third harmonics of the transmit US frequency were filtered out by excluding spectral amplitudes that were within 3 dB with respect to the maximum amplitude at each harmonic. The integrated power spectrum was then calculated across the entire detected frequency range (1-50 MHz) – although the majority of the signal was in the 1-10 MHz range – and then compared to the mean (across all segments) of the integrated FFT of the sham condition (*i.e.*, an ARS without emulsion). Two thresholds related to IC were then calculated. First, the *initiation* of inertial cavitation (IC_L) was defined as the first pressure for which at least one of the 100 segments contained an IC event, which is defined in Eqn. 2

$$S_n\left(P_{i,ARS}\right) > \sum_n^N S_n\left(P_{i,sham}\right)/N + 3\sigma \quad (2)$$

where $S_n(P_{i,ARS})$ is the n^{th} segment in the sequence $P_{i,ARS}$ for an ARS exposed to pressure P_i, $S_n(P_{i,sham})$ is the n^{th} segment in the sequence $P_{i,sham}$ for a sham exposed to pressure P_i, N is the total number of segments, and σ is the standard deviation of the mean of the sham. Second, *persistent* cavitation (IC_H) was defined as the first pressure at which an IC event was detected in all 100 segments, and thus each segment passed the criterion in Eqn. 2.

Viability of encapsulated cells

ARSs were prepared as previously described except that 5.0×10^4 cells/mL of the mouse multipotent line C3H10T1/2, clone 8 (CCL-226, ATCC, Manassas, VA, USA) were encapsulated along with 1% (v/v) PFP double emulsion in 5 mg/mL fibrin. Prior to casting the ARS, OptiCell windows were blocked with a 10 mg/mL solution of BSA. The acoustic exposures (13 cycles and 10 Hz PRF) were completed as previously described except that the single element transducer was rastered across the OptiCell in a paintbrush format to create large regions exposed to the same acoustic condition (rather than a single point as section 2.4). To achieve this, each OptiCell was divided into six equally-sized regions of 500 mm^2, with each region spaced 2 mm from each neighboring region and 5 mm from the edge of the OptiCell window. Each region was exposed to US at a fixed acoustic amplitude. The single element transducer, which was attached to a micropositioning system, was rastered across each region at 0.64 mm/s (i.e., 15 pulses/mm) with a 1 mm spacing between exposure lines. These raster parameters yielded relatively uniform bubble production within the ARS. Immediately after US exposure, the ARS was biopsied with an 8 mm biopsy punch (Miltex, Plainsboro, NJ USA) and each biopsied sample was placed in 0.05% trypsin-EDTA (Gibco, Grand Island, NY USA) for 20 min to degrade the hydrogel. The sham condition (i.e., 0 MPa) was also exposed to the same handling conditions and trypsin degradation as the experimental condition. There was no statistically significant difference in viability when

comparing the sham before and after incubation in trypsin for 20 min. Following complete degradation of the ARS sample, the remaining cells were isolated via centrifugation, resuspended in DMEM, and then stained with 16.2 μM Hoechst 33342 (Invitrogen, Grand Island, NY USA), 5 μM calcein AM ("Live" stain, Invitrogen), and 15 μM propidium iodide (PI, "Dead" stain, Invitrogen). The labeled cells were imaged with a Leica DM IL microscope (Leica Microsystems Inc., Buffalo Groove, IL USA) using a 10× objective.

Physical Stability of ARSs

For stability studies, 0.5 mL ARSs were cast in 24 well plates (Corning Life Sciences, Tewksbury, MA USA) with 1% (v/v) emulsion – either single or double – and 5 mg/mL fibrin. Double emulsions contained 1 mg/mL FSS in the W_1 phase. After polymerization at room temperature, each ARS was covered with DMEM and placed in a standard tissue culture incubator at 37°C. At each time point, the overlying media was removed and the ARS was degraded with 0.05% trypsin-EDTA. Following complete degradation of the ARS, the resulting sample was centrifuged and the remaining emulsion was sized using a Coulter Counter as previously described. It was experimentally confirmed that incubation of the emulsion in trypsin did not alter the size distribution or number density of the emulsion. For studies with double emulsions, the concentration of FSS in the overlying media was determined using a plate reader (Molecular Devices Spectramax M2e, Sunnyvale, CA, USA, 494 nm EX/ 521 nm EM). Measurements were taken twice on the first day at t = 0 h and t = 2 h, then every 24 h from t = 24 h for 144 h. The stability of the emulsions, not contained within ARSs, was also measured using the aforementioned methods. Light microscopy (10× objective, Leica DM IL) images of ARSs containing single PFP and PFH emulsions were taken at t = 0 and t = 72 h to depict differences in physical stability.

Statistics

The data are expressed as the mean ± standard deviation of measured quantities. All *n*-values are listed below each corresponding figure. The Tukey–Kramer method, evaluated in MATLAB, was used to determine statistically significant differences between multiple groups for acoustic data (i.e., ADV and IC thresholds), with differences deemed significant for $p < 0.05$. The 95% confidence interval of slopes is listed in the following format: S [S_L, S_H], where S is the average slope, S_L is the lower bound slope and S_H is the upper bound slope). Statistically significant differences of all other data sets were determined with a Student's *t*-test with differences deemed significant for $p < 0.05$.

Results

Characterization of Emulsions

Table 1 displays the sizing characteristics of the single and double emulsions used in the ARSs. For lipid shell single emulsions, no statistical differences in the mean diameter, droplet concentration, and number percent greater than 6 μm were observed between PFP and PFH emulsions. However, a smaller mean diameter, larger droplet concentration, and a smaller number percent greater than 6 μm were measured when the single PFH emulsions were stabilized with BSA or Pluronic F68 versus lipid. Double emulsion droplets were larger than single emulsions. Additionally, no differences in mean diameter were observed

between double emulsions made with PFP and PFH, however PFP double emulsions had a smaller droplet concentration and larger percentage of droplets greater than 6 μm than PFH double emulsions.

ADV and IC thresholds

Fig. 1B-C display the characteristic trends in ADV and IC of ARSs and sham fibrin scaffolds. At low acoustic pressures, neither bubbles (i.e., ADV) nor IC was detected in the ARS or the sham. As the acoustic pressure was increased, the ADV threshold was reached and the droplets in the ARS started to vaporize, generating echogenic bubbles that increased the MEP in the recorded B-mode images (Fig. 1D). Thus, any acoustic pressure greater than the ADV threshold triggered ADV. A further increase in the acoustic pressure caused the first detectable IC event (i.e., the IC_L threshold), where both IC and ADV occurred. Eventually, at an acoustic pressure higher than the IC_L threshold, persistent IC was detected (i.e., all recorded segments contained at least one IC event). This pressure was the IC_H threshold for an ARS. The acoustic pressure range where IC_H occurred also contained ADV due to detectable bubble formation with B-mode imaging. Sham scaffolds (i.e., fibrin scaffolds without emulsion) did not display an ADV threshold and IC_L occurred at a higher acoustic pressure than the IC_L threshold of an ARS with the same fibrin concentration and exposed to the same number of acoustic cycles. Furthermore IC_H was not detected in any of the sham scaffolds – containing 3, 5, or 10 mg/mL fibrin. Fig. 1D shows a B-mode image of an OptiCell containing an ARS. Fig. 1D-I and Fig. 1D-II shows the ARS before and after US exposure from the single element transducer, respectively. The change in echogenicity (i.e., brightness) post US exposure can be observed, and Fig. 1D-III shows an image subtraction of Fig. 1C-I and 1C-II displaying clear persistent bubble formation and the appearance of the back OptiCell window produced by its shadowing in Fig. 1D-II due to bubble production.

The ADV, IC_L, and IC_H ($IC_{L/H}$) thresholds for an ARS with 5 mg/mL fibrin and doped with varying single emulsion cores (PFP vs. PFH) stabilized by a lipid shell were quantified (Fig. 2A). Qualitatively, all thresholds tended to decrease as the number of acoustic cycles increased, with a statistically significant difference between 3 and 13 cycles for PFH droplets. All thresholds were higher for PFH than PFP at 3 cycles. There were no differences between ADV and IC_L for any acoustic condition in Fig 2-A. However, IC_H was larger than ADV and IC_L for both PFP and PFH at 3 and 6 cycles; at 13 cycles, no differences were observed with the ADV and $IC_{L/H}$ thresholds.

Fig. 2B shows the ADV and $IC_{L/H}$ thresholds for ARSs containing either 3, 5, or 10 mg/mL fibrin and doped with a lipid stabilized, PFH single emulsion. Qualitatively, the ADV and $IC_{L/H}$ thresholds directly correlated with fibrin concentration, with statistically larger ADV and IC_L thresholds at 10 mg/mL versus 3 mg/mL for all acoustic cycles. Similar to the data in Fig. 2A, the ADV and $IC_{L/H}$ thresholds decreased as the number of acoustic cycles increased for 5 and 10 mg/mL fibrin. The IC_H threshold was higher than the ADV and IC_L thresholds for all acoustic conditions and fibrin concentrations except 13 cycles at 3 mg/mL.

The ADV and $IC_{L/H}$ thresholds for ARSs containing 5 mg/mL fibrin and doped with single PFH emulsions of varying droplet shell composition are displayed in Fig. 2C. ARSs doped

with lipid shelled emulsions had a lower IC_L threshold compared to the protein based BSA shell and the polymer based Pluronic F68 shell emulsions at all acoustic cycles, with the largest difference occurring between lipid and Pluronic F68 emulsions. A higher ADV threshold was observed with Pluronic F68 shell emulsions versus lipid shell emulsions at 6 acoustic cycles. For all cases, the IC_H threshold occurred at a higher acoustic pressure than the ADV and IC_L thresholds. Increasing the number of acoustic cycles yielded lower IC_H thresholds for all three shell materials when comparing 3 versus 13 acoustic cycles.

In Fig. 2-D, the ADV and $IC_{L/H}$ thresholds for ARSs containing 5 mg/mL fibrin and doped with either PFP or PFH double emulsions are shown. Similar to the trend observed in Fig. 2-A, PFH emulsions had higher ADV and IC_L thresholds than PFP emulsions when comparing 3 and 6 acoustic cycles. The IC_H threshold was higher than the ADV and IC_L thresholds within all acoustic conditions for PFP emulsions. The IC_L threshold for ARSs doped with PFH double emulsion was equivalent to that observed in the sham. IC_H was not detected with PFH emulsions in the range of acoustic pressures tested.

Cell Viability

The viability of C3H10T1/2 cells encapsulated in an ARS containing 5 mg/mL fibrin and doped with PFP double emulsion was quantified (Fig. 3). This ARS was identical in composition to the ARS in Fig. 2D, with the addition of cells. In Fig. 2D, the ADV, IC_L, and IC_H thresholds occurred approximately at 2, 3.8, and 5 MPa, respectively. The percentage of live cells (i.e., calcein$^+$) correlated inversely with acoustic pressure, with a linear regression of the entire data yielding a slope of −3.2 [−4.7, −1.7]. Conversely, the percentage of dead cells (i.e., PI$^+$) was directly correlated with acoustic pressure, with a linear regression of the entire data yielding a slope of 3.7 [2.2, 5.3]. In the region before ADV and IC (i.e., 0 – 2 MPa), regressions of the live and dead data yield slopes whose 95% confidence intervals are nearly centered at zero (live: −0.1 [−25.8, 25.6], dead: 0.6 [−21.6, 22.8]), thus indicating no change in cell viability. In the region from 0 to 4 MPa, regressions of the live and dead data yield a slope of −0.9 [−5.5, 3.7] for live and 1.6 [−2.9, 6.1] for dead. In the region between 4 and 8 MPa, regressions of the live and dead data yield a slope of −5.7 [−9.5, −1.9] for live and 5.2 [0.3, 10.0] for dead.

Physical stability of ARSs

Light microscopy images of ARSs containing 5 mg/mL fibrin and doped with PFP or PFH double emulsions immediately after and 72 h after polymerization are shown in Fig. 4. These ARSs were not exposed to US and were placed in a standard tissue culture incubator at 37°C between imaging sessions. At 0 h both ARSs contained no bubbles. However after 72 h of incubation, the ARS doped with PFP emulsion contained significantly more bubbles than the ARS doped with PFH emulsion.

Quantification of the physical stability of ARSs containing 5 mg/mL fibrin and doped with single or double emulsions is presented in Fig. 5A-B. The stability is displayed in terms of droplet concentration (i.e., number density per volume of ARS) and volume percentage of droplets remaining. Note that the ARSs initially contained 1% (v/v) emulsion. Fig. 5-A shows the physical stability of ARSs doped with PFP or PFH single emulsions. After 2h,

ARSs doped with PFH single emulsion exhibited a 10% decrease in droplet concentration. After 144 h, a 40% decrease in droplet concentration, relative to 0 h, was observed for the ARS with PFH emulsion. The volume percentage increased to 1.4% after 2 h of incubation and decreased to 1.2% after 144 h of incubation. For ARSs with PFP single emulsions there was a statistically significant decrease in both droplet concentration and volume percentage beginning 24 h after incubation, relative to 0 h, with further decreases in both metrics over time. At 144 h, the droplet concentration and volume percentage decreased by 97% and 94%, respectively, compared to 0 h. No statistically significant differences in mean diameter or number percent greater than 6 μm was observed for ARSs with single PFP or PFH emulsions (data not shown). As a comparison, Supplemental Fig. 1A shows the stability of the same single emulsion formulations in DMEM, at the same concentration used in the ARSs (i.e., 1% (v/)). Overall, droplet concentration and volume percentage of emulsions did not change at 144 h relative to 0 h for PFP and PFH emulsions.

Fig. 5B show that ARSs containing PFP double emulsion exhibited a 50% decrease in droplet concentration 24 hours after polymerization. The concentration then remained relatively unchanged through the remainder of the experiment, with a linear regression of the PFP droplet concentration data yielding a slope roughly centered at zero [-2.8×10^6 , 3.5×10^6]. A 61% decrease in droplet concentration was observed when comparing 0 h versus 144 h. The volume percentage also decreased after 24 hours and remained relatively constant at 0.5%, with a linear regression through the data yielding a slope of 0.001 [−0.001, 0.003]. A 68% decrease in volume percentage was observed when comparing 0 h versus 144 h. This is similar to the results observed in Fig. 5-A where the ARSs doped with PFP single emulsion exhibited a statistically significant decrease in both volume percentage and droplet concentration at 144 h relative to 0 h. For ARS with PFH double emulsion, both the droplet concentration and volume percentage of droplets increased with time. A 27% increase in droplet concentration and a 238% increase in volume percentage was seen when comparing data at 0 h and 144 h. No statistically significant differences in mean diameter or number percent greater than 6 μm was observed for ARSs with double PFP or PFH emulsions (data not shown). Supplemental Fig. 1B shows the stability of double emulsions in DMEM. Similar to single emulsions in DMEM, the droplet concentration and volume percent of emulsions did not decrease at t = 144 h relative to t = 0 h for PFP or PFH emulsions. For PFH double emulsions, the volume percentage increased to 2% (v/v).

Non-selective payload release

The release of FSS from ARSs containing 5 mg/mL fibrin and doped with PFP or PFH double emulsions is shown in Fig. 6. The FSS was initially encapsulated within the W_1 phase of each emulsion. The data in Fig. 6 was acquired in the same experiment as the stability data in Fig. 5. As a control, the release profile of FSS, not encapsulated in a double emulsion but incorporated directly into the fibrin scaffold, is also shown. After 144 h, less than 3% of the initially loaded FSS is released from the ARSs with either the PFP or PFH emulsions. Comparatively, 62% of the initially loaded FSS was released from the control scaffold after 144 h.

Discussion

Recently, we demonstrated that US can be used to actively control GF release, architecture, and stiffness in a fibrin scaffold doped with sonosensitive emulsion (Fabiilli et al. 2013). Here we characterize the acoustic response of fibrin-based ARSs with a surrogate payload and relate it to cell viability within the scaffold, while also focusing on the stability of the ARSs. By design, an ARS is more responsive to US than a conventional fibrin scaffold. The results demonstrated that stable bubbles were created via ADV in all tested compositions of ARSs. For acoustic measurements, all ARSs and sham hydrogels were formulated with degassed DMEM and placed in a degassed water tank, which decreased the amount of dissolved gas present and thus likelihood for bubble generation and persistence within the scaffolds. Bubble formation was not detected in the sham scaffolds (i.e., no droplets) using B-mode US. Additionally, IC_L, and IC_H thresholds were lower in the ARSs, compared to the sham scaffold, except in the case of ARS doped with PFH double emulsions at 3 and 6 cycle pulses (Fig. 2D). This is consistent with previous studies, where the IC threshold of a solution containing microbubbles or high concentrations of dissolved gas was lower than the IC threshold in the same solution without microbubbles or a low concentration of dissolved gas (Fabiilli et al. 2009). During IC, the rapid collapse of cavitation nuclei typically results in various remnant fragments (Flynn and Church 1984; Brennen 2002; Pishchalnikov et al. 2008). These daughter nuclei last from milliseconds to full seconds (Epstein and Plesset 1950; Chen et al. 2002; Pishchalnikov et al. 2008), and may serve as cavitation nuclei for following US pulses. However in degassed media, more aggressive acoustic conditions are required to form cavitation nuclei and any subsequent daughter nuclei. *In vitro* and *in vivo* bioeffects related to IC have been found to correlate with the IC dose, which is the magnitude of IC activity over time (Hallow et al. 2006; Hwang et al. 2006). Thus, for delivery of large molecules such as GFs that have higher order structure, avoidance of acoustic pressures that generate persistent IC may be beneficial in retaining GF bioactivity (Marchioni et al. 2009).

A trend observed in prior work was that the ADV threshold occurred at a lower acoustic pressure than the IC_L threshold, where the bubbles generated by ADV were hypothesized to undergo IC (Fabiilli et al. 2009; Schad and Hynynen 2010). These previous studies measured the acoustic thresholds of sonosensitive emulsions in flowing saline, thus emulating the presence of intravascularly administered emulsion in blood flow. Depending on the flow velocity and acoustic parameters, bubbles generated by ADV may not be insonified by multiple pulses of US. However, bubbles formed in the ARSs are relatively stationary and thus are exposed to multiple acoustic pulses. Therefore, given that 100 pulses were fired at one location within the ARS (Fig. 2), a bubble formed by ADV within the first 99 pulses fired by the single element transducer has the potential to undergo IC during the remaining pulse, at a given acoustic pressure.

ARSs doped with PFH double emulsions displayed higher ADV and $IC_{L/H}$ thresholds than ARSs doped with PFP double emulsions (Fig. 2A versus Fig. 2D). Interestingly, ARSs doped with PFP or PFH single emulsions displayed similar thresholds. Previous studies have demonstrated that the acoustic pressure required to vaporize a PFC emulsion was related to the boiling point of the PFC (Kawabata et al. 2005; Fabiilli et al. 2009; Sheeran et al. 2011).

However another study showed that the IC thresholds of PFC emulsions was independent of the boiling point of the dispersed PFC phase (Giesecke and Hynynen 2003). Gases are very soluble in PFCs, especially oxygen, with the solubility inversely correlated to PFC molecular weight (Riess 2001; Dias et al. 2004; Johnson et al. 2009). It is hypothesized that the interaction of US with the dissolved gases within a PFC droplet causes the vaporization of high boiling point PFCs, such as perfluoro-15-crown-5-ether (boiling point: 146 °C) (Rapoport et al. 2011) or yields similar IC threshold for PFCs with different molecular weights (Giesecke and Hynynen 2003). Thus, the similar ADV thresholds in ARSs with single PFP and PFH emulsions may potentially be attributed in part to high gas solubility within both PFCs.

For the same number of acoustic cycles, ARSs doped with double emulsions generally displayed higher ADV and $IC_{L/H}$ thresholds than ARSs doped with single emulsions (Fig. 2A versus Fig. 2D). These acoustic differences could be due to variations in the outer shell stabilizing the emulsion droplets, droplet diameter, or emulsion morphology. The outer shells of the single and double emulsions were lipid and Pluronic F68, respectively. It can be seen in Fig. 2C that ARSs containing single emulsions with Pluronic F68 shells had higher acoustic thresholds than ARSs with single emulsions with lipid shells. Since the ADV threshold is inversely related to droplet size (Fabiilli et al. 2009; Schad and Hynynen 2010; Sheeran et al. 2011), it was expected that the ADV threshold of ARSs with double emulsions would have been lower than single emulsions since the double emulsions were larger in size (Table 1). Thus, it is hypothesized that the mechanism governing the initiation of ADV for double emulsions is different than that of single emulsions. In addition, the fraction of PFC within a double emulsion droplet is smaller than in a single emulsion droplet, which may diminish the probability for an appropriate nucleation site and therefore increase the pressure needed to trigger ADV in a double emulsion. Prior work has also shown that the expansion rate of double emulsions is slower than that of single emulsions during ADV (Shpak et al. 2013). Thus more acoustic energy may be required to displace the viscous hydrogel media surrounding the double emulsion droplet while also preventing recondensation of the PFC during the relatively slow expansion.

For ARSs with single emulsions, the effects of shell material and droplet size on ADV and $IC_{L/H}$ thresholds cannot be completely decoupled since different shells yielded differently sized emulsions. As stated previously, higher thresholds were observed with Pluronic F68 emulsions versus lipid shell emulsions (Fig. 2C). Microbubbles with a soft-shell surfactant, such as lipid, can undergo net radial fluctuations of at least 15%, while stiffer albumin-shelled microbubbles demonstrate constrained expansion and contraction when exposed to US (Dayton et al. 1999). In addition, microbubbles with stiffer polymer based shells have higher fragmentation thresholds than lipid-based microbubbles (Chen et al. 2003). Lipid shell emulsions also displayed the largest mean diameter and highest percentage of droplets greater than 6 μm, which could also lead to a lower ADV and $IC_{L/H}$ thresholds. Within an ARS, the interaction between a droplet and the surrounding fibrin could be affected by the physiochemical properties of the shell stabilizing the droplet. For example, Pluronic F68 can alter the arrangement of fibrin fibers, which could ultimately impact the acoustic response of the ARS (Vangelder et al. 1993). Such interactions would also explain the apparent instability of the PFP droplets in the ARSs in comparison to that found in aqueous solutions.

In addition, the ADV thresholds of single emulsions within the ARS could be modified by altering surfactant composition, which has been shown to influence the interfacial tension of PFC and aqueous solutions (Kandadai et al. 2010).

With conventional fibrin scaffolds, the rate of cellular infiltration and the extent of neovascularization are inversely related to fibrin density (Kniazeva et al. 2011). In this study, higher ADV and IC thresholds were observed as the fibrin concentration of the ARS increased. The inertia of the surrounding media, large Laplace pressure, and viscosity may delay the startup of bubble nucleation during ADV or growth during ADV/IC. If the time delay caused by these factors comprise a significant portion of the acoustic period, then a much higher acoustic pressure could be required to initiate the growth of the bubble from the emulsion or to cause the generated bubble to undergo IC (Apfel 1986; Holland and Apfel 1989; Fabiilli et al. 2009; Fabiilli et al. 2013). Overall, ADV and IC thresholds generally decreased as the number of acoustic cycles increased. Previous research has demonstrated an inverse correlation between the IC threshold and the number of acoustic cycles, especially in the range of 1 to 10 cycles (Atchley et al. 1988; Fowlkes and Crum 1988; Ammi et al. 2006).

Since the ADV and IC thresholds can be modulated by altering the composition of the ARS, this opens the possibility of expanding the therapeutic capabilities of an ARS beyond what has been previously demonstrated (Fabiilli et al. 2013). US could be used to modulate the porosity or mechanical properties of ARSs containing single emulsions to influence cell invasion into the ARS. Alternatively, single emulsions could be used to deliver therapeutic gases within the ARS (Faithfull 1992). Release of two distinct payloads could be achieved by formulating an ARS with two different double emulsion formulations. For example, as seen in Fig. 2-D, the ADV thresholds in an ARS containing PFP or PFH double emulsion is 2.5 MPa and 3 MPa, respectively, at 3 cycles. Therefore one payload could be released first at the lower acoustic threshold while a second payload could be released at a higher acoustic threshold – thus enabling temporal control of multiple payload release. Though not investigated in this work, the use of different US frequencies could also be used to tune different release thresholds (Kripfgans 2002; Schad and Hynynen 2010; Martz et al. 2011). Other modifications to the droplet formulations including differential size distributions could further increase the separation in threshold for temporal control. Spatial control of ADV/IC and payload release is also an inherent feature of an ARS due to the use of focused US as the means to interact with the sonosensitive emulsion, compared to studies where unfocused US has been used to facilitate drug release (Huebsch et al. 2014). The use of megahertz frequency US to trigger ADV enables patterning at submillimeter resolution within an ARS. Additionally, ADV thresholds of the ARSs ranged from approximately 1.5 to 3 MPa peak rarefactional pressure, which is within the output range of clinical diagnostic US scanners (i.e., at 2.5 MHz, 3 MPa is equivalent to a mechanical index of 1.9 which is the current upper limit set by the United States Food and Drug Administration). Clinically-approved, therapeutic US systems, typically operating in the 1-3 MHz range, could be used to generate ADV at higher acoustic pressures within an ARS.

Cell adherence and viability can be impacted by US capable of generating ADV and IC. ADV adjacent to adherent cells can cause detachment (Ohl et al. 2006) while an 80%

decrease in cell number was observed for cells in the presence of bubbles undergoing IC (Ward et al. 1999). It was previously demonstrated that the viability of cells encapsulated in an ARS was not impacted by high amplitude US used to generate ADV within an ARS, when measured 2 days after ADV exposure (Fabiilli et al. 2013). However, this prior study investigated only one acoustic condition (i.e., 6 MPa peak rarefactional pressure at 3.5 MHz, MI = 3.2) and the presence of IC was not measured. In this work, the viability of cells contained in the ARS was not affected by acoustic pressures up to 2 MPa but decreased to 60% when exposed to an acoustic pressure of 8 MPa, which generated sustained IC. As seen in Fig. 2, some of the ADV thresholds occurred at pressures less than 2 MPa. Additionally, the use of higher frequency US could reduce the acoustic bioeffects stemming from IC, though at the expense of depth penetration. Beyond viability, the impact of ADV and IC on cellular proliferation, differentiation, apoptosis, as well as cytokine production in an ARS are also critically important, but were outside of the scope of this work.

The physical stability of the emulsion used to dope an ARS is relevant to the stability of the ARS as a whole and can impact the ability of US to interact with the ARS. ARSs doped with PFH emulsions displayed less spontaneous (i.e., in the absence of US) bubble formation than ARSs doped with PFP emulsions. The millimeter size bubbles formed in the ARS doped with PFP likely formed via coalescence of multiple smaller bubbles. Also, subsequent in-gassing may have occurred as the ARS, which was prepared with degassed fluids, was placed into a cell culture incubator at atmospheric gas saturation with 5% carbon dioxide. Additional nucleation of dissolved gas within the PFC could also have occurred as the ARS warmed from room temperature to 37°C. It is hypothesized that the higher boiling point of PFH versus PFP imparts greater stability. Previous studies with PFP emulsions indicate that these droplets are stable at 37°C (Fabiilli et al. 2013), though few if any studies explored the stability at 37°C for one week or in a matrix like a fibrin scaffold. Additionally, as seen when comparing Fig. 5 to Supplemental Fig. 1B, PFP emulsions displayed greater stability in DMEM versus in an ARS. Within an ARS, the fibrin surrounding each droplet may be exerting tension on the droplet, or effectively lowering the interfacial tension, which would destabilize the PFC droplet.

Encapsulation of FSS within the W_1 phase of the emulsion hindered its release from the ARS when compared to non-emulsified FSS (Fig. 6). However, despite exhibiting greater stability, the retention of FSS was similar for ARSs doped with PFP and PFH double emulsions. The higher bubble density within ARSs doped with PFP double emulsion could impact the diffusivity of FSS through the ARS. Overall, the greater stability of the ARS with PFH double emulsion makes this composition better suited for controlled release or *in vivo* implantation since any spontaneously formed bubbles would prevent US from penetrating the ARS. In additional to spontaneous vaporization, the population of PFC droplets may be shifting toward larger sizes, due to droplet coalescence or Ostwald ripening. This would cause sub-micron size droplets that are initially below the sizing range of the Coulter Counter to enter the detectable range (i.e., 1 – 30 μm), thus causing an increase in the droplet concentration and volume percentage. The osmotic imbalance between the W_1 phase, which contained FSS at 1 mg/mL, and the surrounding environment (*i.e.*, the fibrin scaffold and

overlying DMEM), could have contributed to the increase in volume percentage of the emulsion within the ARS doped with PFH double emulsion.

Conclusions

In this study, we characterized the interactions of US with droplets and associated bubbles occurring in sonosensitive hydrogels. ADV and IC thresholds were modulated by modifying ARS parameters such as fibrin concentration, emulsion shell material, PFC core, emulsion structure, and the number of acoustic cycles. ADV occurred within an ARS with minimal effects on cell viability while IC caused decreases in viability. ARSs doped with PFH emulsions displayed better physical stability and less spontaneous bubble formation than ARSs doped with PFP emulsions. Non-selective payload release was minimal for both ARS compositions tested. Based on this study, the recommended ARS composition for GF delivery consists of 5 or 10 mg/mL fibrin with a double emulsion containing PFH or an admixture of PFP/PFH. For the US exposure, a higher number of acoustic cycles is also recommended.

Supplementary Material

Refer to Web version on PubMed Central for supplementary material.

Acknowledgements

This work was supported by NIH grant R21AR065010 (MLF) and the Basic Radiological Sciences Innovative Research Award (MLF). AM is supported by the National Science Foundation Graduate Student Research Fellowship (Grant No. DGE 1256260).

References

Ammi AY, Cleveland RO, Mamou J, Wang GI, Bridal SL, O'Brien WD. Ultrasonic contrast agent shell rupture detected by inertial cavitation and rebound signals. Ieee Transactions on Ultrasonics Ferroelectrics and Frequency Control. 2006; 53:126–36.

Apfel RE. POSSIBILITY OF MICROCAVITATION FROM DIAGNOSTIC ULTRASOUND. Ieee Transactions on Ultrasonics Ferroelectrics and Frequency Control. 1986; 33:139–42.

Apfel RE, Holland CK. Gauging the likelihood of cavitation from short-pulse, low-duty cycle diagnostic ultrasound. Ultrasound in Medicine and Biology. 1991; 17:179–85. [PubMed: 2053214]

Atchley AA, Frizzell LA, Apfel RE, Holland CK, Madanshetty S, Roy RA. Thresholds for Cavitation Produced in Water by Pulsed Ultrasound. Ultrasonics. 1988; 26:280–5. [PubMed: 3407017]

Barthes J, Ozcelik H, Hindie M, Ndreu-Halili A, Hasan A, Vrana NE. Cell Microenvironment Engineering and Monitoring for Tissue Engineering and Regenerative Medicine: The Recent Advances. Biomed Research International. 2014

Bos PK, van Osch GJVM, Frenz DA, Verhaar JAN, Verwoerd-Verhoef HL. Growth factor expression in cartilage wound healing: temporal and spatial immunolocalization in a rabbit auricular cartilage wound model. Osteoarthritis and Cartilage. 2001; 9:382–9. [PubMed: 11399103]

Brennen CE. Fission of collapsing cavitation bubbles. Journal of Fluid Mechanics. 2002; 472:153–66.

Chen WS, Matula TJ, Brayman AA, Crum LA. A comparison of the fragmentation thresholds and inertial cavitation doses of different ultrasound contrast agents. Journal of the Acoustical Society of America. 2003; 113:643–51. [PubMed: 12558300]

Chen WS, Matula TJ, Crum LA. The disappearance of ultrasound contrast bubbles: Observations of bubble dissolution and cavitation nucleation. Ultrasound Med Biol. 2002; 28:793–803. [PubMed: 12113792]

Dayton PA, Morgan KE, Klibanov AL, Brandenburger GH, Ferrara KW. Optical and acoustical observations of the effects of ultrasound on contrast agents. Ieee Transactions on Ultrasonics Ferroelectrics and Frequency Control. 1999; 46:220–32.

Dehghani F, Annabi N. Engineering porous scaffolds using gas-based techniques. Current Opinion in Biotechnology. 2011; 22:661–6. [PubMed: 21546240]

Dias AMA, Freire M, Coutinho JAP, Marrucho IM. Solubility of oxygen in liquid perfluorocarbons. Fluid Phase Equilibria. 2004; 222:325–30.

Diaz-Lopez R, Tsapis N, Fattal E. Liquid perfluorocarbons as contrast agents for ultrasonography and 19F-MRI. Pharmaceutical Research. 2010; 27:1–16. [PubMed: 19902338]

Epstein PS, Plesset MS. On the stability of gas bubbles in liquid-gas solutions. Journal of Chemical Physics. 1950; 18:1505–9.

Epstein-Barash H, Orbey G, Polat BE, Ewoldt RH, Feshitan J, Langer R, Borden MA, Kohane DS. A microcomposite hydrogel for repeated on-demand ultrasound-triggered drug delivery. Biomaterials. 2010; 31:5208–17. [PubMed: 20347484]

Fabiilli ML, Haworth KJ, Fakhri NH, Kripfgans OD, Carson PL, Fowlkes JB. The role of inertial cavitation in acoustic droplet vaporization. IEEE Trans Ultrason Ferroelectr Freq Control. 2009; 56:1006–17. [PubMed: 19473917]

Fabiilli ML, Lee JA, Kripfgans OD, Carson PL, Fowlkes JB. Delivery of water-soluble drugs using acoustically triggered perfluorocarbon double emulsions. Pharm Res. 2010; 27:2753–65. [PubMed: 20872050]

Fabiilli ML, Wilson CG, Padilla F, Martin-Saavedra FM, Fowlkes JB, Franceschi RT. Acoustic droplet-hydrogel composites for spatial and temporal control of growth factor delivery and scaffold stiffness. Acta Biomaterialia. 2013

Faithfull NS. OXYGEN DELIVERY FROM FLUOROCARBON EMULSIONS - ASPECTS OF CONVECTIVE AND DIFFUSIVE TRANSPORT. Biomaterials Artificial Cells and Immobilization Biotechnology. 1992; 20:797–804.

Ferrara KW, Pollard R, Borden MA. Ultrasound microbubble contrast agents: fundamentals and application to gene and drug delivery. Annual Review of Biomedical Engineering. 2007; 9:425–47.

Flynn HG, Church CC. A MECHANISM FOR THE GENERATION OF CAVITATION MAXIMA BY PULSED ULTRASOUND. Journal of the Acoustical Society of America. 1984; 76:505–12. [PubMed: 6481000]

Fowlkes JB, Crum LA. CAVITATION THRESHOLD MEASUREMENTS FOR MICROSECOND LENGTH PULSES OF ULTRASOUND. Journal of the Acoustical Society of America. 1988; 83:2190–201. [PubMed: 3411016]

Frimpong RA, Fraser S, Hilt JZ. Synthesis and temperature response analysis of magnetic-hydrogel nanocomposites. Journal of Biomedical Materials Research Part A. 2007; 80A:1–6. [PubMed: 16941587]

Fujie T, Mori Y, Ito S, Nishizawa M, Bae H, Nagai N, Onami H, Abe T, Khademhosseini A, Kaji H. Micropatterned Polymeric Nanosheets for Local Delivery of an Engineered Epithelial Monolayer. Advanced Materials. 2014; 26:1699–705. [PubMed: 24307219]

Giesecke T, Hynynen K. Ultrasound-mediated cavitation thresholds of liquid perfluorocarbon Droplets \textitin vitro. Ultrasound in Medicine and Biology. 2003; 29:1359–65. [PubMed: 14553814]

Hallow DM, Mahajan AD, McCutchen TE, Prausnitz MR. Measurement and correlation of acoustic cavitation with cellular bioeffects. Ultrasound in Medicine and Biology. 2006; 32:1111–22. [PubMed: 16829325]

Holland CK, Apfel RE. An improved theory for the prediction of microcavitation thresholds. IEEE Transactions on Ultrasonics, Ferroelectrics, and Frequency Control. 1989; 36:204–8.

Huebsch N, Kearney CJ, Zhao XH, Kim J, Cezar CA, Suo ZG, Mooney DJ. Ultrasound-triggered disruption and self-healing of reversibly cross-linked hydrogels for drug delivery and enhanced chemotherapy. Proceedings of the National Academy of Sciences of the United States of America. 2014; 111:9762–7. [PubMed: 24961369]

Hwang JH, Tu J, Brayman AA, Matula TJ, Crum LA. Correlation between inertial cavitation dose and endothelial cell damage in vivo. Ultrasound in Medicine and Biology. 2006; 32:1611–9. [PubMed: 17045882]

Javadi M, Pitt WG, Tracy CM, Barrow JR, Willardson BM, Hartley JM, Tsosie NH. Ultrasonic gene and drug delivery using eLiposomes. Journal of Controlled Release. 2013; 167:92–100. [PubMed: 23352908]

Johnson JLH, Dolezal MC, Kerschen A, Matsunaga TO, Unger EC. In vitro comparison of dodecafluoropentane (DDFP), perfluorodecalin (PFD), and perfluoroctylbromide (PFOB) in the facilitation of oxygen exchange. Artificial cells, blood substitutes, and biotechnology. 2009; 37:156–62.

Kandadai MA, Mohan P, Lin G, Butterfield A, Skliar M, Magda JJ. Comparison of surfactants used to prepare aqueous perfluoropentane emulsions for pharmaceutical applications. Langmuir. 2010; 26:4655–60. [PubMed: 20218695]

Kawabata K-I, Sugita N, Yoshikawa H, Azuma T, Umemura S-I. Nanoparticles with Multiple Perfluorocarbons for Controllable Ultrasonically Induced Phase Shifting. Japanese Journal of Applied Physics. 2005; 44:4548–52.

Kniazeva E, Kachgal S, Putnam AJ. Effects of Extracellular Matrix Density and Mesenchymal Stem Cells on Neovascularization In Vivo. Tissue Engineering Part A. 2011; 17:905–14. [PubMed: 20979533]

Kripfgans OD, Fabiilli ML, Carson PL, Fowlkes JB. On the acoustic vaporization of micrometer-sized droplets. J Acoust Soc Am. 2004; 116:272–81. [PubMed: 15295987]

Kripfgans OD, Fowlkes JB, Miller DL, Eldevik OP, Carson PL. Acoustic droplet vaporization for therapeutic and diagnostic applications. Ultrasound in Medicine and Biology. 2000; 26:1177–89. [PubMed: 11053753]

Kulkarni R, Biswanath S. Electrically responsive smart hydrogels in drug delivery: a review. Journal of Applied Biomaterials and Biomechanics. 2007; 5:125–39. [PubMed: 20799182]

Lavigne MD, Pennadam SS, Ellis J, Yates LL, Alexander C, Gorecki DC. Enhanced gene expression through temperature profile-induced variations in molecular architecture of thermoresponsive polymer vectors. The Journal of Gene Medicine. 2007; 9:44–54. [PubMed: 17167816]

Lima EG, Durney KM, Sirsi SR, Nover AB, Ateshian GA, Borden MA, Hung CT. Microbubbles as biocompatible porogens for hydrogel scaffolds. Acta Biomaterialia. 2012 in press.

Madanshetty SI, Apfel RE. ACOUSTIC MICROCAVITATION - ENHANCEMENT AND APPLICATIONS. Journal of the Acoustical Society of America. 1991; 90:1508–14. [PubMed: 1939907]

Marchioni C, Riccardi E, Spinelli S, dell'Unto F, Grimaldi P, Bedini A, Giliberti C, Giuliani L, Palomba R, Castellano AC. Structural changes induced in proteins by therapeutic ultrasounds. Ultrasonics. 2009; 49:569–76. [PubMed: 19278707]

Martz TD, Sheeran PS, Bardin D, Lee AP, Dayton PA. Precision Manufacture of Phase-Change Perfluorocarbon Droplets Using Microfluidics. Ultrasound in Medicine and Biology. 2011; 37:1952–7. [PubMed: 21963036]

Matsusaki M, Akashi M. Novel functional biodegradable polymer IV: pH-Sensitive controlled release of fibroblast growth factor-2 from a poly(gamma-glutamic acid)-sulfonate matrix for tissue engineering. Biomacromolecules. 2005; 6:3351–6. [PubMed: 16283765]

Meijering BDM, Henning RH, Van Gilst WH, Gavrilovic I, Van Wamel A, Deelman LE. Optimization of ultrasound and microbubbles targeted gene delivery to cultured primary endothelial cells. Journal of Drug Targeting. 2007; 15:664–71. [PubMed: 18041634]

Metallo CM, Mohr JC, Detzel CJ, de Pablo JJ, Van Wie BJ, Palecek SP. Engineering the stem cell microenvironment. Biotechnology Progress. 2007; 23:18–23. [PubMed: 17269664]

Nair A, Thevenot P, Dey J, Shen JH, Sun MW, Yang J, Tang LP. Novel Polymeric Scaffolds Using Protein Microbubbles as Porogen and Growth Factor Carriers. Tissue Engineering Part C-Methods. 2010; 16:23–32. [PubMed: 19327002]

Ohl C-D, Arora M, Ikink R, de Jong N, Versluis M, Delius M, Lohse D. Sonoporation from jetting cavitation bubbles. Biophysical Journal. 2006; 91:4285–95. [PubMed: 16950843]

Pishchalnikov YA, McAteer JA, Pishchalnikova IV, Williams JC, Bailey MR, Sapozhnikov OA. Enflo BO, Hedberg CM, Kari L. Bubble proliferation in shock wave lithotripsy occurs during inertial collapse. Nonlinear Acoustics Fundamentals and Applications. 2008:460–3.

Rahim A, Taylor SL, Bush NL, Ter Haar GR, Bamber JC, Porter CD. Physical parameters affecting ultrasound/microbubble-mediated gene delivery efficiency in vitro. Ultrasound in Medicine and Biology. 2006a; 32:1269–79. [PubMed: 16875960]

Rahim AA, Taylor SL, Bush NL, ter Haar GR, Bamber JC, Porter CD. Spatial and acoustic pressure dependence of microbubble-mediated gene delivery targeted using focused ultrasound. Journal of Gene Medicine. 2006b; 8:1347–57. [PubMed: 16981246]

Rapoport N, Nam KH, Gupta R, Gao ZG, Mohan P, Payne A, Todd N, Liu X, Kim T, Shea J, Scaife C, Parker DL, Jeong EK, Kennedy AM. Ultrasound-mediated tumor imaging and nanotherapy using drug loaded, block copolymer stabilized perfluorocarbon nanoemulsions. Journal of Controlled Release. 2011; 153:4–15. [PubMed: 21277919]

Rapoport NY, Kennedy AM, Shea JE, Scaife CL, Nam K-H. Controlled and targeted tumor chemotherapy by ultrasound-activated nanoemulsions/microbubbles. Journal of Controlled Release. 2009; 138:268–76. [PubMed: 19477208]

Riess JG. Oxygen Carriers ("Blood Substitutes") - Raison d'Etre, Chemistry, and Some Physiology. Chemical Reviews. 2001; 101:2797–919. [PubMed: 11749396]

Sakiyama-Elbert SE, Hubbell JA. Controlled release of nerve growth factor from a heparin-containing fibrin-based cell ingrowth matrix. Journal of Controlled Release. 2000a; 69:149–58. [PubMed: 11018553]

Sakiyama-Elbert SE, Hubbell JA. Development of fibrin derivatives for controlled release of heparin-binding growth factors. Journal of Controlled Release. 2000b; 65:389–402. [PubMed: 10699297]

Satyam A, Kumar P, Fan XL, Gorelov A, Rochev Y, Joshi L, Peinado H, Lyden D, Thomas B, Rodriguez B, Raghunath M, Pandit A, Zeugolis D. Macromolecular Crowding Meets Tissue Engineering by Self-Assembly: A Paradigm Shift in Regenerative Medicine. Advanced Materials. 2014; 26:3024–34. [PubMed: 24505025]

Schad KC, Hynynen K. In vitro characterization of perfluorocarbon droplets for focused ultrasound therapy. Physics in Medicine and Biology. 2010; 55:4933–47. [PubMed: 20693614]

Seliktar D. Designing Cell-Compatible Hydrogels for Biomedical Applications. Science. 2012; 336:1124–8. [PubMed: 22654050]

Shaikh FM, Callanan A, Kavanagh EG, Burke PE, Grace PA, McGloughlin TM. Fibrin: A natural biodegradable scaffold in vascular tissue engineering. Cells Tissues Organs. 2008; 188:333–46. [PubMed: 18552484]

Sheeran PS, Wong VP, Luois S, McFarland RJ, Ross WD, Feingold S, Matsunaga TO, Dayton PA. Decafluorobutane as a Phase-Change Contrast Agent for Low-Energy Extravascular Ultrasonic Imaging. Ultrasound in Medicine and Biology. 2011; 37:1518–30. [PubMed: 21775049]

Shpak O, Stricker L, Kokhuis T, Luan Y, Fowlkes B, Fabiilli M, Lohse D, de Jong N, Versluis M. Ultrafast dynamics of the acoustic vaporization of phase-change microdroplets. The Journal of the Acoustical Society of America. 2013; 133:3586.

Sojo K, Sawaki Y, Hattori H, Mizutani H, Ueda M. Immunohistochemical study of vascular endothelial growth factor (VEGF) and bone morphogenetic protein-2,-4 (BMP-2,-4) on lengthened rat femurs. Journal of Cranio-Maxillofacial Surgery. 2005; 33:238–45. [PubMed: 15979317]

Thornton PD, McConnell G, Ulijn RV. Enzyme responsive polymer hydrogel beads. Chemical Communications. 2005:5913–5. [PubMed: 16317473]

Tse HTK, Weaver WM, Di Carlo D. Increased Asymmetric and Multi-Daughter Cell Division in Mechanically Confined Microenvironments. Plos One. 2012:7.

Unger EC, Porter T, Culp W, LaBell R, Matsunaga T, Zutshi R. Therapeutic applications of lipid-coated microbubbles. Advanced Drug Delivery Reviews. 2004; 56:1291–314. [PubMed: 15109770]

Vangelder JM, Nair CH, Dhall DP. EFFECTS OF POLOXAMER-188 ON FIBRIN NETWORK STRUCTURE, WHOLE-BLOOD CLOT PERMEABILITY AND FIBRINOLYSIS. Thrombosis Research. 1993; 71:361–76. [PubMed: 8236163]

Ward M, Wu JR, Chiu JF. Ultrasound-induced cell lysis and sonoporation enhanced by contrast agents. Journal of the Acoustical Society of America. 1999; 105:2951–7. [PubMed: 10335644]

Whelan D, Caplice NM, Clover AJP. Fibrin as a delivery system in wound healing tissue engineering applications. Journal of Controlled Release. 2014; 196:1–8. [PubMed: 25284479]

Wong ZZ, Kripfgans OD, Qamar A, Fowlkes JB, Bull JL. Bubble evolution in acoustic droplet vaporization at physiological temperature via ultra-high speed imaging. Soft Matter. 2011; 7:4009–16.

Wu C, Chen C, Lai J, Mu X, Zheng J, Zhao Y. Molecule-scale controlled-release system based on light-responsive silica nanoparticles. Chemical Communications. 2008; 23:2662–4. [PubMed: 18535700]

Zhao X, Kim J, Cezar CA, Huebsch N, Lee K, Bouhadir K, Mooney DJ. Active scaffolds for on-demand drug and cell delivery. Proceedings of the National Academy of Sciences of the United States of America. 2011; 108:67–72. [PubMed: 21149682]

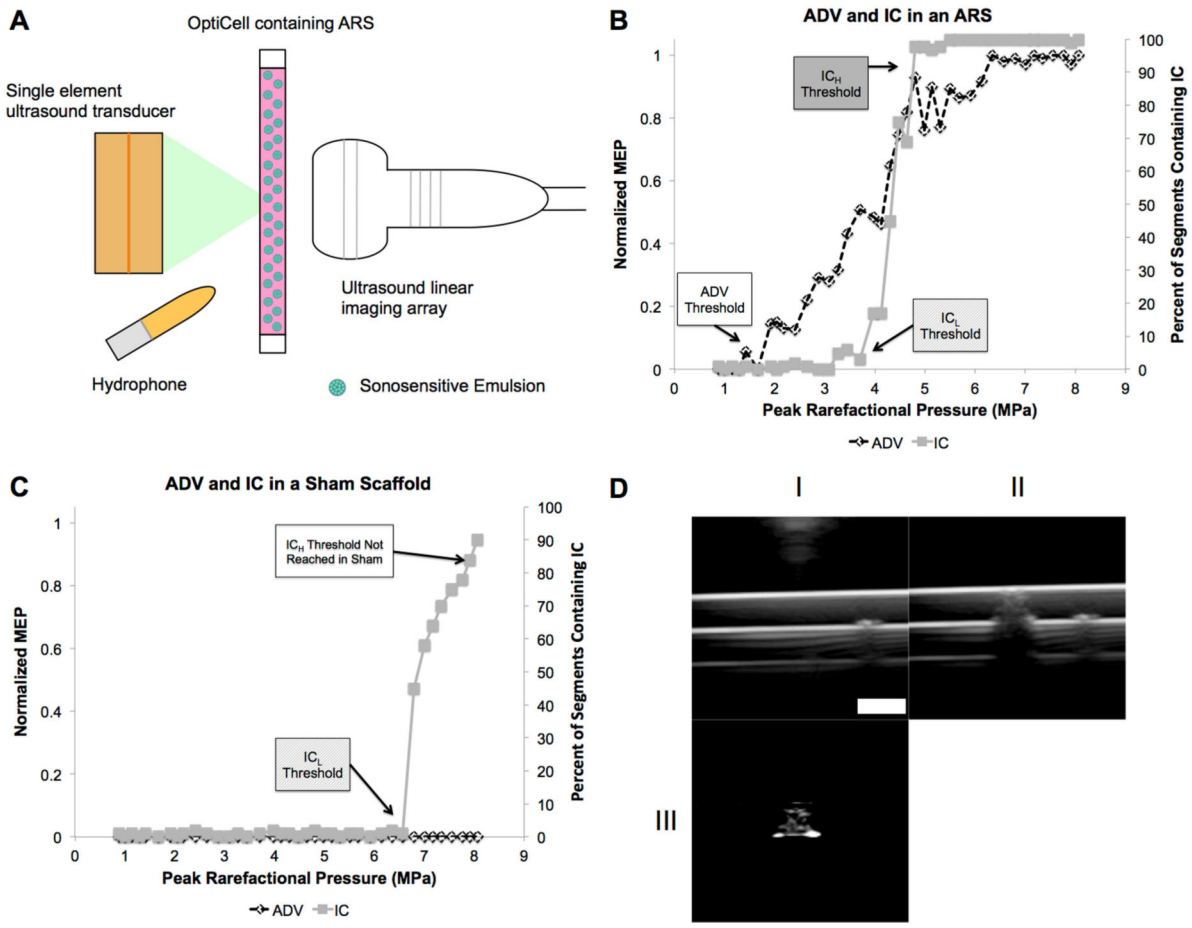

Figure 1.

(A) Experimental setup used to expose ARSs to US. Representative plots showcasing the behavior of ADV, measured via enhanced brightness in the B-mode US images (*i.e.*, MEP), and IC, measured via enhanced broadband noise, for an ARS (B) and a sham scaffold (C, without droplets). The ADV and IC_L thresholds were defined as the first acoustic pressure data point that met the criteria in Equations 1 and 2, respectively. The threshold for persistent cavitation, IC_H, was defined as the first acoustic pressure data point where all 100 segments contained at least one IC event. For the sham scaffold (C), there was no detectable ADV due to the absence of droplets and also no enhanced brightness due to persistent bubbles generated by IC. Additionally, IC_L occurred at a higher acoustic pressure relative to the ARS with the same fibrin concentration. IC_H was not measured in the sham scaffold across the range of acoustic pressures interrogated in this work (i.e., 0 – 8.07 MPa). B-mode US images of the cross-section of an OptiCell containing an ARS (D). Images were taken before (DI) and after (DII) the ARS was exposed to high amplitude acoustic pulses generated by the single element US transducer. The subtracted image of DII – DI (DIII) clearly shows the bubbles generated by ADV in the ARS, which was used for ADV threshold analysis (i.e., MEP). Scale bar = 2 mm.

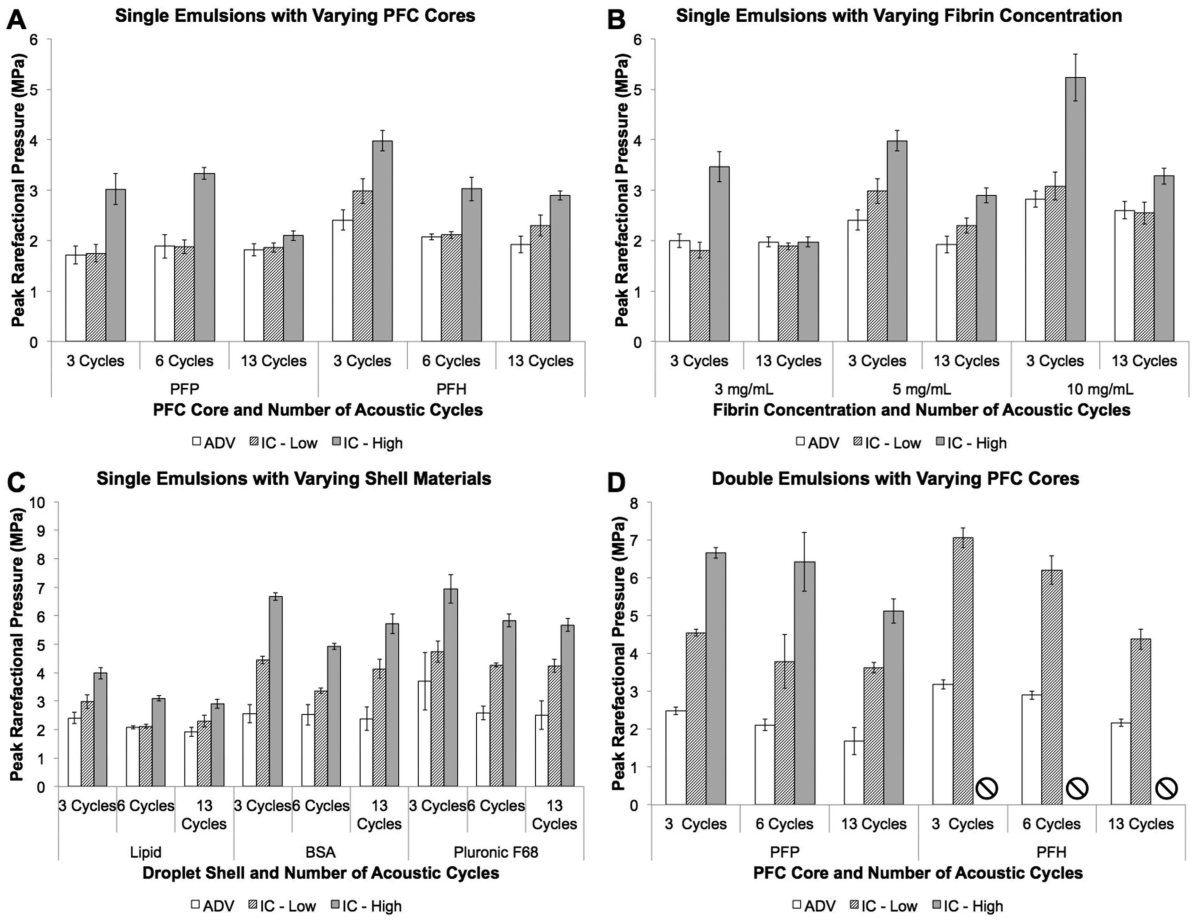

Figure 2.

ADV and IC thresholds of ARSs containing varying (A) droplet formulations (i.e., different PFC cores), (B) fibrin concentration, (C) droplet shell material, and (D) emulsion structures. For each parameter set, the number of acoustic cycles was varied. In (B) and (C), the ARSs were doped with a PFH single emulsion. A fibrin concentration of 5 mg/mL fibrin was used in ARSs in (A), (C), and (D). A lipid shell was used in (A) and (B). For certain conditions in (D), IC_H was not detected in the range of acoustic pressures interrogated in this work (i.e, 0 – 8.07 MPa); these conditions are denoted by an '□'. Data are shown as mean ± standard deviation for n = 5 and all ARSs were prepared the day of acoustic measurement. Statistically significant differences within each subfigure are detailed in Supplemental Tables 1 – 4.

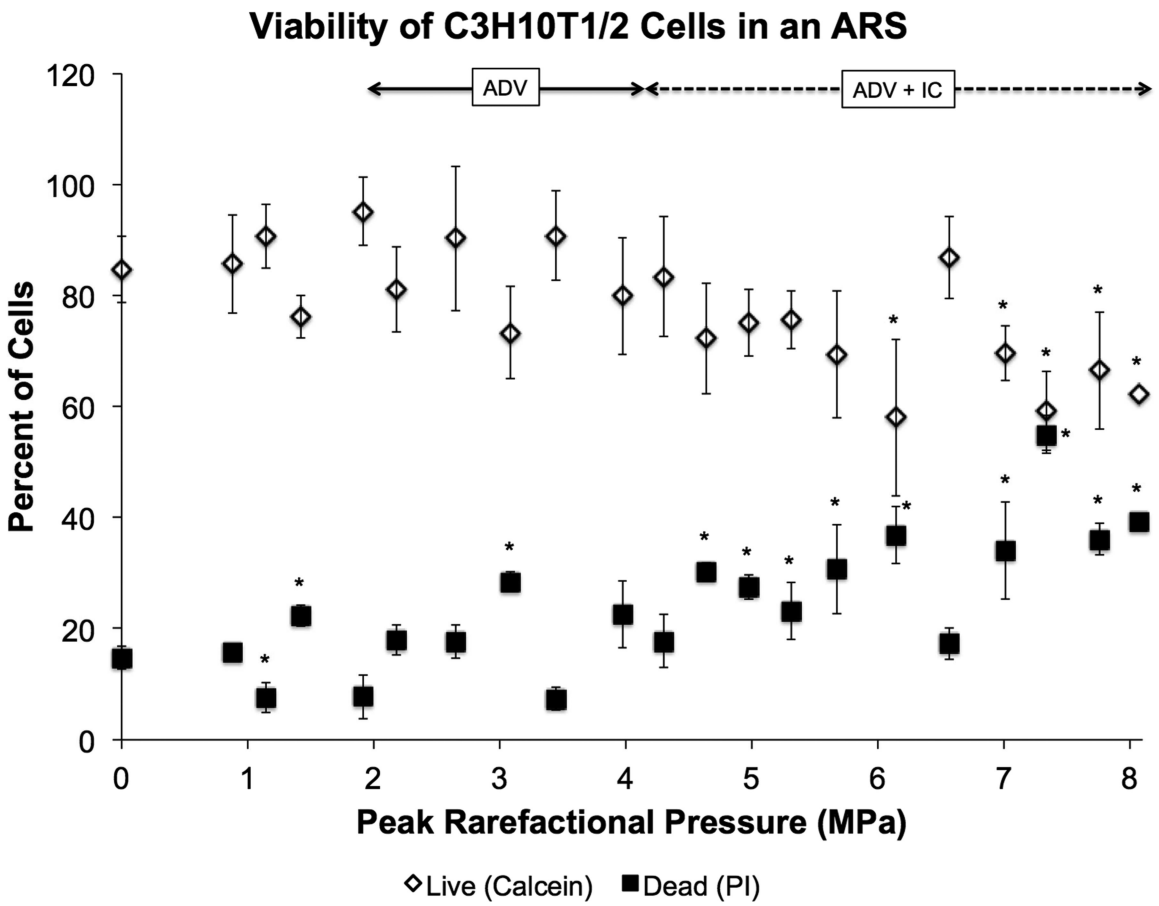

Figure 3.

Viability of C3H10T1/2 cells in an ARS containing 5 mg/mL fibrin, 1% (v/v) PFP double emulsion, and 50,000 cells/mL after exposure to US at 13 cycles and 10 Hz PRF. Viability was determined with calcein for live staining, propidium iodide for dead staining, and Hoechst for total number of cells. The sham condition (i.e., 0 MPa) underwent the same experimental steps and exposure to environmental conditions as the non-sham conditions. Data are shown as mean ± standard deviation for n = 9. *$p < 0.05$ vs. no US condition.

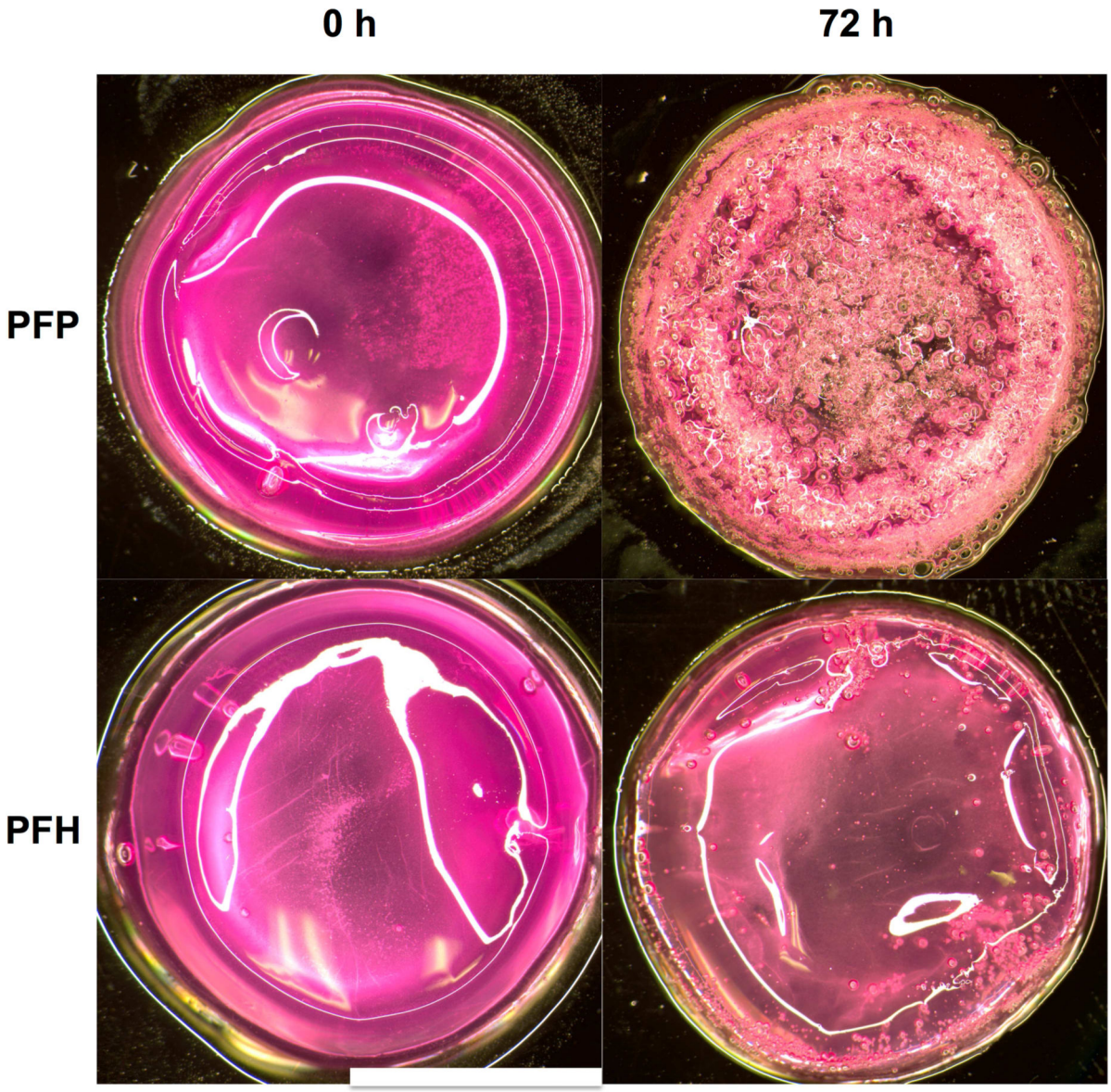

Figure 4.

Light microscopy images of ARSs doped with 1% (v/v) PFP or PFH emulsions at 0 h and 72 h after polymerization. Between imaging, the ARSs were placed in a standard tissue culture incubator at 37°C and were not exposed to U S. Scale bar = 7.8 mm.

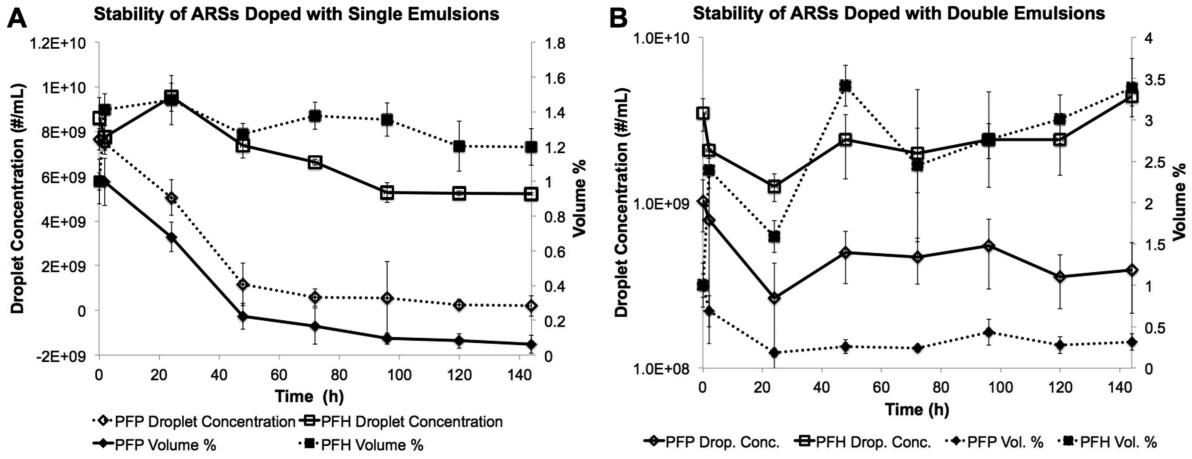

Figure 5.

Physical stability of ARSs doped with single (A) and double (B) emulsions. The ARSs were degraded with 0.05% trypsin and the remaining emulsion was sized with a Coulter Counter. Data are shown as mean ± standard deviation for n = 5.

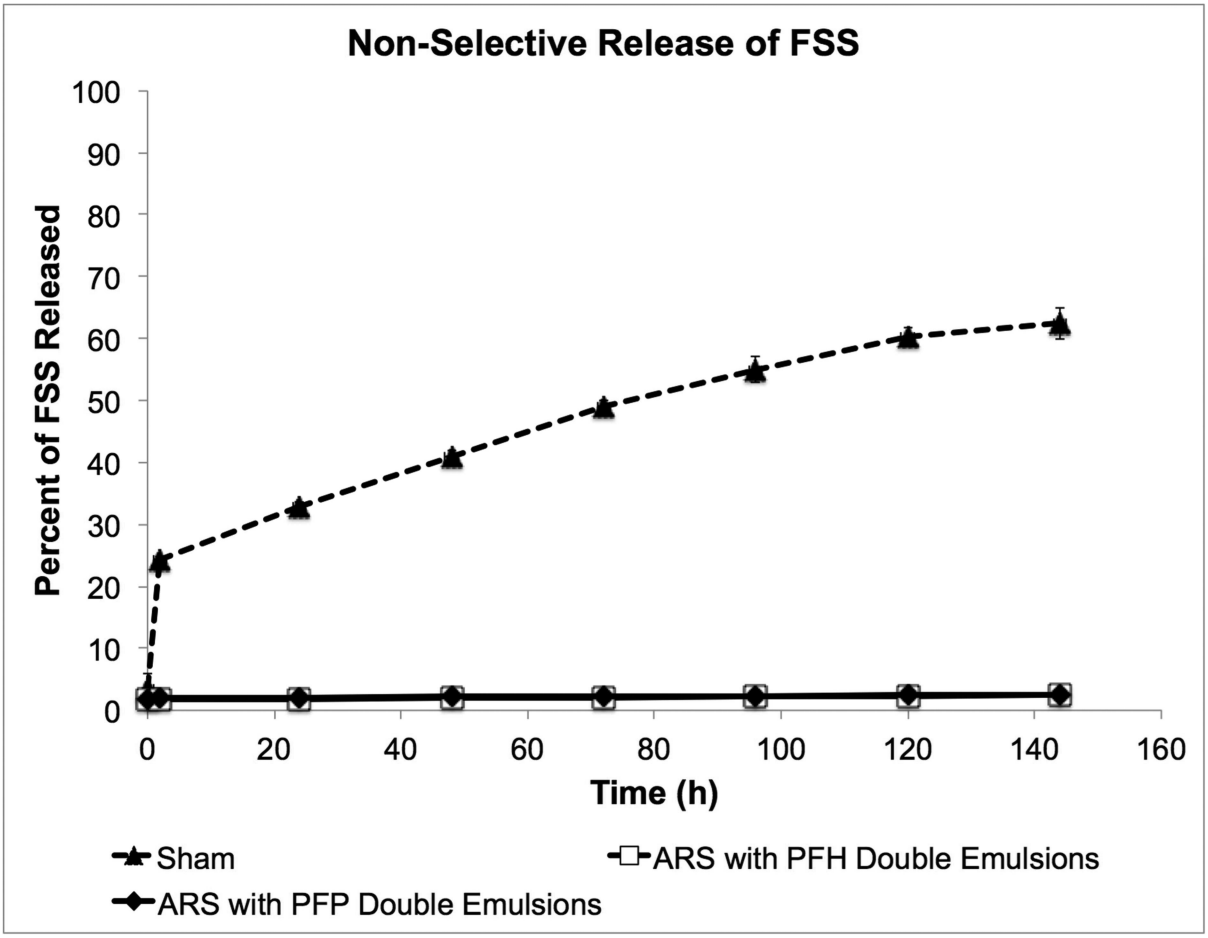

Figure 6.

Non-selective (i.e., without US exposure) release of a small molecular weight surrogate payload, FSS, from ARSs containing PFP or PFH double emulsions. The FSS was encapsulated within the W_1 phases of the respective emulsions. The ARSs were placed in a standard tissue culture incubator at 37°C. The rel ease profile of non-emulsified FSS, doped within a sham fibrin scaffold (i.e., without emulsion) is also shown. Data are shown as mean ± standard deviation for n = 5.

Table 1

Structure and composition of emulsions used to dope the ARSs. Sizing parameters of the emulsions were determined with a Coulter Counter. Data are shown as mean ± standard deviation for n = 3.

Structure	PFC	Shell	Mean Diameter	Mean Diameter St. Dev.	Drop Concentration	Drop Concentration St. Dev.	% > 6 microns	% > 6 microns St. Dev.
Single	PFP	Lipid	2.34	0.08	6.27E+09	1.84E+09	5.99	1.93
Single	PFH	Lipid	2.27	0.04	6.54E+09	1.56E+09	4.78	1.23
Single	PFH	BSA	1.80	0.01	1.98E+10	2.41E+09	1.02	0.05
Single	PFH	Pluronic F68	2.12	0.14	1.03E+10	2.99E+09	1.25	0.18
Double	PFP	Fluoro Surfactant / Pluronic F68	4.95	0.59	5.15E+08	9.67E+07	27.99	2.98
Double	PFH	Fluoro Surfactant / Pluronic F68	4.00	0.22	9.90E+08	3.17E+08	13.03	3.72